THE JOURNAL OF BIOLOGICAL CHEMISTRY VOL. 281, NO. 22, pp. 15145–15154, June 2, 2006

Copper-mediated Amyloid-β Toxicity Is Associated with an Intermolecular Histidine Bridge*[S]

Received for publication, January 17, 2006, and in revised form, March 24, 2006 Published, JBC Papers in Press, April 6, 2006, DOI 10.1074/jbc.M600417200

David P. Smith[‡§1], Danielle G. Smith[‡§], Cyril C. Curtain[‡§¶], John F. Boas[¶], John R. Pilbrow[¶], Giuseppe D. Ciccotosto[‡§], Tong-Lay Lau[‡‖], Deborah J. Tew[‡§], Keyla Perez[‡§], John D. Wade[**], Ashley I. Bush[§‡‡2], Simon C. Drew[§§], Frances Separovic[‖], Colin L. Masters[‡§2], Roberto Cappai[‡§¶¶2], and Kevin J. Barnham[‡§2,3]

From the [‡]Department of Pathology, [¶¶]Centre for Neuroscience, and [‖]School of Chemistry, University of Melbourne, Victoria 3010, Australia, the [§]Mental Health Research Institute of Victoria, Victoria 3010, Australia, the [¶]School of Physics, Monash University, Victoria 3800, Australia, the [**]Howard Florey Institute of Medical Research, Victoria 3010, Australia, the [‡‡]Laboratory for Oxidation Biology, Genetics, and Aging Research Unit, Massachusetts General Hospital, Harvard Medical School, Charlestown, Massachusetts 02129, and the [§§]Centre for Magnetic Resonance and Centre for Metals in Biology, University of Queensland, Queensland 4072, Australia

Amyloid-β peptide (Aβ) is pivotal to the pathogenesis of Alzheimer disease. Here we report the formation of a toxic Aβ-Cu^{2+} complex formed via a histidine-bridged dimer, as observed at Cu^{2+}/peptide ratios of >0.6:1 by EPR spectroscopy. The toxicity of the Aβ-Cu^{2+} complex to cultured primary cortical neurons was attenuated when either the π- or τ-nitrogen of the imidazole side chains of His were methylated, thereby inhibiting formation of the His bridge. Toxicity did not correlate with the ability to form amyloid or perturb the acyl-chain region of a lipid membrane as measured by diphenyl-1,3,5-hexatriene anisotropy, but did correlate with lipid peroxidation and dityrosine formation. ^{31}P magic angle spinning solid-state NMR showed that Aβ and Aβ-Cu^{2+} complexes interacted at the surface of a lipid membrane. These findings indicate that the generation of the Aβ toxic species is modulated by the Cu^{2+} concentration and the ability to form an intermolecular His bridge.

The interaction of metals with the amyloid-β peptide (Aβ)[4] plays a pivotal role in the pathogenesis of Alzheimer disease (AD). Transition metals, such as copper (Cu^{2+}), zinc (Zn^{2+}), and iron (Fe^{3+}), are enriched in Aβ plaques (1), and the Aβ peptide possesses both high and low affinity Cu^{2+} and Zn^{2+} binding sites *in vitro*. These interactions with Cu^{2+}, Zn^{2+}, and to a lesser extent Fe^{3+} have been reported to control the aggregation state of Aβ. Moreover, the Aβ-Cu^{2+} complexes are redox-active, suggesting that the oxidative stress observed in AD patients is related to the production of reactive oxygen species (ROS) by metal-bound forms of Aβ and may be central to the pathological mechanism of AD (reviewed by Bush (1)).

The coordination environment of Cu^{2+} bound to Aβ has been studied by EPR, Raman, and NMR spectroscopies. The consensus is that the coordination of Cu^{2+} to Aβ is via the three His residues His^6, His^{13}, and His^{14} and an as yet undefined fourth ligand; options put forward include tyrosine (Tyr^{10}) (2–6), the N-terminal nitrogen (7), or an as yet unidentified carboxylate side chain (8, 9) (Fig. 1*a*). Recently, Glu^{11} has been identified as providing the carboxylate side chain when Zn^{2+} is bound to Aβ 1–16 (10). The EPR studies of Curtain *et al.* (2) showed that in the pH range 6.0 to 7.5 in PBS, an increase in the Cu^{2+}/peptide molar ratio above ~0.3:1 broadened the mononuclear Cu^{2+} spectrum observed at low ratios. At Cu^{2+}/peptide molar ratios greater than 0.6:1, a distinctive broad resonance developed near g ~ 2. This broad resonance was attributed to exchange interactions between two Cu^{2+} ions ~6 Å apart, with the second Cu^{2+} ion being coordinated to Aβ in a cooperative manner via a His bridge (Fig. 1*b*), similar to that observed by Ohtsu *et al.* (11) for Cu^{2+} bridge imidizolate complexes. Here we report the first observation of resonances at g ~ 4 in the EPR spectra of Aβ-Cu^{2+} peptides, where the broad g ~ 2 line is also observed. Such EPR spectra are diagnostic for the existence of binuclear Cu^{2+} centers where the Cu^{2+} ions are coupled by dipolar interactions; simulations presented here demonstrate that these atoms are 6.2 ± 0.2 Å apart (12). This distance is consistent with a His bridge between the Cu^{2+} atoms. To further the understanding of the role played by the His bridge and Aβ-lipid interactions in the neurotoxicity of Aβ, we examine the toxic mechanism of both metal-free and Cu^{2+}-bound forms of the Aβ peptide.

The link between His bridge formation and neurotoxicity was explored through experiments using Aβ 1-42 peptides modified by the methylation of the His residues at either the π- or τ-nitrogen of the imidazole side chain (Fig. 1*c*). Correspondingly modified Aβ 1-40 has been shown to be nontoxic, despite being redox-active in a manner similar to the wild type (WT) peptide (4). This lack of toxicity has been attributed to these peptides being unable to bind to cell surface membranes, congruent with the notion that Aβ-lipid membrane interactions are central to the cause of neurotoxicity in AD (13–17). Here we describe the Cu^{2+} coordination, lipid interactions, and aggregation properties of both the neurotoxic WT Aβ 1-42 peptide and Aβ 1-42 where the His residues have been methylated at either the π- or τ-nitrogen of the imidazole side chain. The Cu^{2+}-bound WT Aβ 1-42 peptide was shown to be significantly more toxic, as monitored by the viability of primary cortical neurons, under conditions in which the His bridge was formed. Perturbation of this metal coordination mode leads

* This work was supported in part by the Wellcome Trust, National Health and Medical Research Council of Australia, Australian Research Council, and Prana Biotechnology Ltd. The costs of publication of this article were defrayed in part by the payment of page charges. This article must therefore be hereby marked "*advertisement*" in accordance with 18 U.S.C. Section 1734 solely to indicate this fact.

[S] The on-line version of this article (available at http://www.jbc.org) contains supplemental Table 1 and Figs. 1–3.

[1] A Wellcome Travelling Fellow.

[2] Consultant to Prana Biotechnology Ltd.

[3] To whom correspondence should be addressed: Dept. of Pathology, University of Melbourne, Victoria 3010, Australia. Tel.: 61-3-8344-1805; Fax: 61-3-8344-4004; E-mail: kbarnham@unimelb.edu.au.

[4] The abbreviations used are: Aβ, amyloid peptide; PC, 1-palmitoyl-2-oleoyl-*sn*-glycero-3-phosphocholine; PS, 1-palmitoyl-2-oleoyl-*sn*-glycero-3-[phospho-L-serine]; His-π-Me, amyloid peptide 1-42 where the His residues have been methylated at π-nitrogen of the imidazole side chain; His-τ-Me, amyloid peptide 1-42 where the His residues have been methylated at τ-nitrogen of the imidazole side chain; AD, Alzheimer disease; CQ, clioquinol; DPH, diphenyl-1,3,5-hexatriene; HFIP, hexaflouro-2-propanol; LUVs, large unilamellar vesicles; ROS, reactive oxygen species; PBS, phosphate-buffered saline; ThT, thioflavin-T; WT, wild type; Fmoc, *N*-(9-fluorenyl)methoxycarbonyl; MTS, 3-(4,5,-dimethylthiazol-2-yl)-5-(3-carboxymethoxyphenyl)-2-(4-sulfophenyl)-2H-tetrazolium, inner salt.

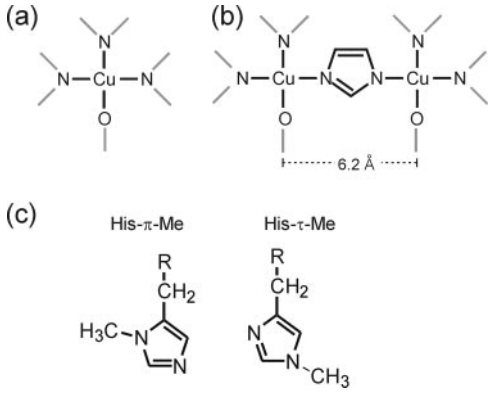

FIGURE 1. **Illustration of Cu^{2+} coordination by Aβ.** *a*, N3O coordination about the Cu^{2+} is supplied by the imidazole nitrogens of the three His side chains (His^6, His^{13}, and His^{14}) and a yet to be identified oxygen atom. *b*, the imidazole side chain of a His residue bridging between Cu^{2+} atoms generating Aβ dimer and a metal coordination site similar to the active site of SOD 1 (25). *c*, methylation of the imidazole side chain of His at either the π or τ position, designed to allow the initial copper binding event to occur but inhibit the subsequent formation of His-bridged structures.

to a loss in toxicity even in the presence of Cu^{2+}. We also show that toxicity correlates with the ability of the peptides to form dityrosine and induce lipid peroxidation. Toxicity displays a negative correlation with the formation of amyloid material and the ability to perturb the acyl-chain region of lipid bilayer. These results show that the ability to form a Cu^{2+}-linked His bridge dimer, resulting ultimately in lipid peroxidation, is central to the metal-meditated toxicity of Aβ.

EXPERIMENTAL PROCEDURES

All reagents were purchased from Sigma unless otherwise stated.

Peptide Synthesis—The uncommon N^{im}-protected amino acids, Fmoc-L-His(*N*-1-Me)-OH (His-π-Me) and Fmoc-L-His(*N*-3-Me)-OH (His-τ-Me), were purchased from Bachem (Bubendorf, Switzerland); all were used without further purification. All modified peptides were synthesized according to methods outlined previously (18). Due to the large degree of similarity between the peptides, large batches of resins were prepared and split at appropriate points in the synthetic pathway such that each peptide was prepared on a scale of 0.03 mmol. WT Aβ 1-42 was purchased from the W. M. Keck Laboratory (Yale University, New Haven, CT).

Peptide and Aggregate Preparation—PBS is defined as 10 mM sodium phosphate, 150 mM NaCl at pH 7.4. Cu^{2+} was present as a solution of 1 part $CuCl_2$ to 6 parts glycine. The addition of a glycine counterion was essential in order to prevent the formation of insoluble phosphate-metal complexes. A 25 mM stock solution was made and diluted in deionized water to the desired concentration as required. Peptide working solutions were prepared by taking a known amount of Aβ 1-42 and then dissolving it in 1,1,1,3,3,3-hexafluoro-2-isopropanol (HFIP). The peptide was incubated at 25 °C for 1 h to remove any preformed structure. Known amounts of peptide were then aliquoted out, and HFIP was removed by evaporation. The resulting peptide film was stored at −80 °C until required. The film was dissolved in 20 mM NaOH and then diluted out in deionized water and 10× PBS at a v/v/v ratio of 2:7:1. All solutions were sonicated in a water bath for 10 min and centrifuged for 10 min at 4 °C at high speed before the addition of 10× PBS. The supernatant was kept on ice for immediate use. The absorbance value at 214 nm was measured, and the concentration of the peptides was determined using a molar extinction coefficient value of 75,887 liters/mol/cm, adjusting to the required concentration with buffer A. $CuCl_2$/Gly was added to the required concentration from a 25 mM stock. Samples were used immediately or incubated at 37 °C with agitation at 200 rpm for either 2 or 24 h.

EPR Spectroscopy—Continuous wave EPR spectra were obtained with Bruker ESP380E FT/CW and ECS106 X-band spectrometers. Temperatures around 120 K in both were achieved with a Bruker nitrogen gas flow insert in the standard rectangular TE_{012} cavity. Spectra acquired at 2.5 K using the ESP380E were achieved using an Oxford Instruments CF935 cryostat with an ER4118 cylindrical cavity insert. The microwave frequency was measured with an EIP microwave 548A frequency counter, and the g factors were determined with reference to the F^+ line in CaO (19). Spectrum simulations were performed with the SOPHE software (version 1.1.4) described by Hanson *et al.* (20). For the EPR measurements, the chloride of 99.99% pure ^{65}Cu (Cambridge Isotopes) was used. The peptides were dissolved from an HFIP-treated stock to 100 μM in deionized water, and $^{65}CuCl_2$ to the desired Cu^{2+}/peptide molar ratio was added immediately from a 2.0 mM stock solution via a glass microsyringe. The pH was then adjusted to 7.4 by adding concentrated PBS or ethylmorpholine buffer, and after mixing, samples were rapidly transferred to Wilmad "Suprasil" EPR tubes and frozen immediately. Before and after the EPR spectroscopy, metal concentrations were measured by inductively coupled plasma mass spectrometry, and peptide concentrations were determined by quantitative amino acid analysis.

High Performance Immobilized Metal Ion Chromatography—All solutions were delivered to the column at a flow rate of 1.5 ml/min. The high performance immobilized metal ion chromatography column (Amersham Biosciences) was swollen in PBS (pH 7.4), washed in EDTA (50 mM) to remove trace metals, and then washed with deionized H_2O. The column was charged with Cu^{2+} by injecting 2 ml of 0.1 M $CuCl_2$/glycine(1:6). The excess metal was removed by washing the column with deionized H_2O. The column was then re-equilibrated in PBS (15 ml). The peptides were prepared at 1 mM in 10% 2′,2′,2′-trifluoroethanol/PBS, and 5 μl was injected onto the column. The peptides were eluted using either a pH gradient (7.4–2.5) generated by a linear increase (0–100%) in PBS at pH 2.5 or an imidazole gradient (0–100% 500 mM imidazole in PBS at pH 7.4).

Primary Neuronal Cultures—Cortical neuronal cultures were prepared as described previously (21). Briefly, embryonic day 14 BL6Jx129sv mouse cortices were removed, dissected free of meninges, and dissociated in 0.025% (w/v) trypsin in Krebs buffer. The dissociated cells were triturated using a filter-plugged fine pipette tip, pelleted, resuspended in plating medium (minimum Eagle's medium, 10% fetal calf serum, 5% horse serum), and counted. Cortical neuronal cells were plated into poly(L-lysine)-coated 48-well plates at a density of 125,000 cells/well in plating medium. All cultures were maintained in an incubator set at 37 °C with 5% CO_2. After 2 h, the plating medium was replaced with fresh neurobasal medium containing B_{27} supplements, Geneticin, and 0.5 mM glutamine (all tissue culture reagents were purchased from Invitrogen unless otherwise stated). This method resulted in cultures highly enriched for neurons (>95% purity) with minimal astrocyte and microglial content as determined by immunostaining of culture preparations using specific marker antibodies.

Cell Viability Assay—The neuronal cells were allowed to mature for 6 days in culture before commencing treatment using freshly prepared serum free neurobasal medium plus B_{27} supplements minus antioxidants. For the treatment of neuronal cultures, peptide was prepared at 50 μM at Cu^{2+}/peptide molar ratios of 0:1, 0.1:1, 1:1, and 10:1 and used immediately. Peptides were diluted to the final concentration of 5 μM in neurobasal medium. The mixtures were then added to neuronal cells for 96 h. Cell survival was monitored by phase-contrast microscopy, and cell viability was quantitated using the MTS assay as described previously (21). Briefly, the medium was replaced with fresh neurobasal

medium supplemented with B_{27} lacking antioxidants, and 10% (v/v) MTS (Promega, Madison, WI) was added to each well and incubated for 3 h at 37 °C in a 5% CO_2 incubator. Plates were gently shaken, and a 150-μl aliquot from each well was transferred to separate wells of a 96-well plate. The color change of each well was determined by measuring the absorbance at 490 nm using a Wallac Victor Multireader, and background readings of MTS incubated in cell-free medium were subtracted from each value before calculations. The data were normalized and calculated as a percentage of untreated vehicle control values. Data are shown as mean ± S.E. Statistical comparisons between groups were done using Student's *t* test.

Quantification of Aggregate and Fibril Formation—For determination of fibril growth end points, a discontinuous assay of fibril growth was used. Peptide samples (20 μl) were removed from incubation after 2 or 24 h and added to 600 μl of a 20 μM thioflavin-T (ThT) solution at pH 7.4 in buffer A. The ThT signal was quantified by averaging the fluorescence emission at 480 nm over 10 s when excited at 444 nm using a PerkinElmer Life Sciences LS55 fluorescence spectrophotometer, slit widths for excitation of 2.5 nm and emission of 12.5 nm at 37 °C.

Circular Dichroism Spectroscopy—The peptides were prepared as described above diluting to a final concentration of 20 μM in PBS to achieve a measurable CD signal. Cu^{2+} was titrated into the peptide preparation at 0.5–2.5 peptide mol eq after diluting the peptide, gently mixed, and allowed to equilibrate for 15 min at room temperature. Far UV-CD spectra were collected between 200 and 250 nm at room temperature on a Jasco 810 spectrometer using a quartz cuvette with a 1-cm path length. Measurements were recorded at 50 nm/min with a bandwidth of 1 nm and a response time of 2 s, averaging 10 accumulation scans per measurement. The spectra were background-subtracted, smoothed using the Jasco software (version 32) FFT filter function, and converted to molar ellipticity. All experiments were performed in triplicate.

Dityrosine Formation—Peptide was prepared at 10 μM in the presence of 250 μM H_2O_2 at Cu^{2+}/peptide molar ratios of 1:1. After 24 h of incubation, the reaction was quenched by the addition of 10 μl of 12.5 mM EDTA (final concentration 250 μM). Dityrosine content was quantified using a PerkinElmer Life Sciences LS55 fluorescence spectrophotometer with an excitation wavelength of 320 nm and scanning the emission wavelengths from 350 to 500 nm. Maximum light signal was observed and recorded at 418 nm (22).

Preparation of Large Unilamellar Vesicles—Large unilamellar vesicles (LUVs) were prepared by initially dissolving equal quantities of 1-palmitoyl-2-oleoyl-*sn*-glycero-3-phosphocholine (PC) and 1-palmitoyl-2-oleoyl-*sn*-glycero-3-[phospho-L-serine] (PS) (Avanti Polar Lipids Inc.) in chloroform. The chloroform was evaporated off, and the lipids were resuspended in buffer A at ~10 mM and incubated at 37 °C for 1 h with agitation at 200 rpm in the presence of glass beads. The lipid mixture was subjected to five freeze-thaw cycles using liquid nitrogen and a 37 °C water bath. The sample was then passed through an extruder apparatus using a 100-nm filter, resulting in a uniform solution of LUVs with a mean diameter between 120 and 140 nm.

Steady-state Polarization of DPH—Diphenyl-1,3,5-hexatriene (DPH) was purchased from Molecular Probes. Briefly, DPH was dissolved at 10 mM in Me_2SO and diluted to 16.6 μM in buffer A containing 416 μM LUVs. A 60-μl aliquot of this sample was mixed with 40 μl of Aβ 1-42 at 10 μM, giving final concentrations of 10 μM probe, 250 μM LUVs, and 4 μM peptide. Samples were then incubated at 37 °C with aggregation at 200 rpm for 20 min prior to reading. The dye was excited at 359 nm, and emission was recorded at 430 nm. Anisotropy was measured on a Varian Eclipses spectrophotometer using internal polarizers and calculated by the equation, $r = (Ivv - G{\cdot}Ivh)/(Ivv + 2G{\cdot}Ivh)$, where *Ivv* and *Ivh* are the fluorescence intensities when the excitation and emission polarizers are set at *v* (vertical) and *h* (horizontal), respectively. The grating factor $G = Ihv/Ihh$.

Solid-state NMR—Solid-state NMR experiments were conducted on a Varian Inova 300 spectrometer operating at a resonance frequency of 121.4 MHz for ^{31}P. ^{31}P spectra were acquired at 28 °C, using a Doty 5-mm double resonance NMR probe with a standard Hahn echo and proton decoupling. Pulse times used were $\pi/2 = 5$ μs pulse with a delay of 2 s under magic angle spinning of ~5 kHz. Typically, 10,000 scans were acquired, and an exponential line broadening of 10 Hz was applied. Chemical shift was referenced using 80% phosphoric acid (H_3PO_4) as 0 ppm for ^{31}P NMR experiments.

Lipid Peroxidation—20 μM peptide was prepared as above at a Cu^{2+}/peptide molar ratio of 0:1 or 1:1. Samples were incubated for 5 min before the addition to 50% PC, 50% PS LUVs and ascorbate. Samples contained a final concentration of 10 μM peptide, 1 mM LUV, and 10 μM ascorbate and were incubated for 24 h at 37 °C with agitation at 200 rpm. CQ was prepared in 100% Me_2SO and added to final concentrations of 2, 20, and 50 μM. The final Me_2SO concentration was 1% in all cases. The level of lipid peroxidation was quantified via a lipid peroxidation colorimetric assay (Oxford Biomedical Research) as per the manufacturer's instructions.

RESULTS

The His Bridge Dimer as Observed by EPR—Most of the experiments described below were performed at pH 7.4 in PBS solutions, because NaCl at a concentration of ~0.15 M is part of the physiological milieu. Under these conditions of pH, peptide concentration, and buffer, the predominant species observed by EPR depended on the Cu^{2+}/peptide molar ratio. The addition of $^{65}CuCl_2$ to Aβ 1–16, Aβ 1–28, and WT Aβ 1-42 to give Cu^{2+}/peptide molar ratios of 0–0.5:1 gave EPR signals analogous to that shown in Fig. 2*a*. These spectra are similar to those reported previously (2, 3) for low Cu^{2+}/peptide ratios and show a spectrum mainly due to mononuclear Cu^{2+} in an approximately axially symmetric square planar environment. A simulated spectrum using the spin-Hamiltonian parameters is given in supplemental Table 1. These parameters are typical for Cu^{2+} coordinated by 2N2O or 3N1O (23).

At Cu^{2+}/peptide molar ratios of above 0.5:1, a significantly different resonance developed in the g ~ 2 region, as reported previously (2, 4) and as shown in Fig. 2*b*. Concurrently, we demonstrate here for the first time that a resonance also develops at g ~ 4 when very high spectrometer gains are used (Fig. 3). The parallel appearance of the g ~ 2 and g ~ 4 resonances is diagnostic for the existence of a binuclear Cu^{2+} center (*i.e.* a pair of Cu^{2+} ions coupled by exchange and/or dipolar interactions) (12). Although the Cu^{2+} hyperfine structure is not well resolved, its presence is confirmation that the resonance at g ~ 4 is due to a pair of Cu^{2+} ions and not to a nonspecific aggregate. At Cu^{2+}/peptide molar ratios of ~1:1 and greater, another broad resonance developed centered at g ~ 2.14 (Fig. 2*c*). No resonance at g ~ 4 appears to be associated with this new signal, which may be attributed to a number of Cu^{2+} ions within ~10 Å of each other but not structurally related. The *broken line spectrum* in Fig. 2*c* represents the simulation of an isotropic resonance at g ~ 2.14, such as might arise from a number of Cu^{2+} ions within ~10 Å of each other without a specific geometrical relationship and where the anisotropic features are averaged by a combination of dipolar and weak exchange interactions.

Spectra acquired at 2.5 K of Aβ 1–28 (Cu^{2+}/peptide molar ratio 1:1) exhibited the same resonances as observed at 120 K at g ~ 2 and g ~ 4 but with 50 times the intensity, indicating that antiferromagnetic

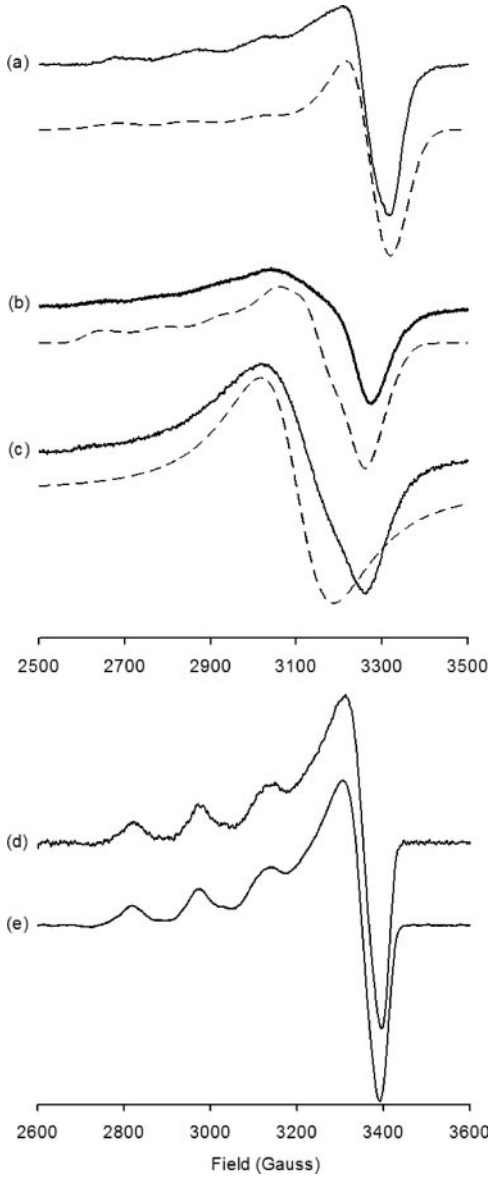

FIGURE 2. **EPR spectra of Aβ 1-28 and Aβ 1-42 at varying Cu^{2+}/peptide molar ratios.** *Top*, EPR spectra of Aβ 1-28 at Cu^{2+}/peptide molar ratios 0.3:1 (*a*), 0.6:1 (*b*), and 1:1 (*c*) in PBS, pH 7.4, at 120 K. Spectrometer and settings were as follows: Bruker ESP380E, microwave frequency 9.424 GHz, microwave power 1.05 milliwatts, modulation frequency 100 kHz, modulation amplitude 1.0 G, receiver gain 5×10^4, scan time 84 s, time constant 84 ms, single scan. *Broken lines*, SOPHE simulations (20) of the predominant species in the corresponding spectrum. Spin-Hamiltonian parameters are given in supplemental Table 1. *Bottom*, EPR spectrum of Aβ 1-42 at a Cu^{2+}/peptide molar ratio of 0.1:1 (*d*) compared with the spectrum of His-τ-Me at a Cu^{2+}/peptide molar ratio of 1:1 (*e*) in PBS, pH 7.4, at 120 K. Spectrometer and settings were as follows: Bruker ECS106, 9.71 GHz, microwave power 5.05 milliwatts, modulation frequency 100 kHz, modulation amplitude 5.0 G, receiver gain 5×10^5, scan time 84 s, time constant 40 ms, nine scans.

exchange interactions between the Cu^{2+} ions of the dimer must be $\ll 10\ cm^{-1}$. The dimer spectra did not exhibit microwave power saturation up to 25 milliwatts at 2.5 K, indicating the existence of spin-spin relaxation processes as expected for a coupled system. In contrast, the mononuclear spectra exhibited power saturation effects above ~1 milliwatt at 2.5 K. To verify that the g ~ 2 and g ~ 4 spectra were not due to oxo- or phosphate-bridged binuclear Cu^{2+} centers or to adventitious Fe^{3+}, control spectra were acquired at 120 K of 1.5 mM $^{65}CuCl_2$ in PBS, of PBS alone, and of the peptide in PBS prior to the addition of $^{65}CuCl_2$. At pH 7.4, no resonances were observed near either g ~ 2 or g ~ 4.

As a comparison with WT Aβ 1-42, the spectra of Aβ 1-42 containing His-τ-Me or His-π-Me at positions 6, 13, and 14 were recorded over the

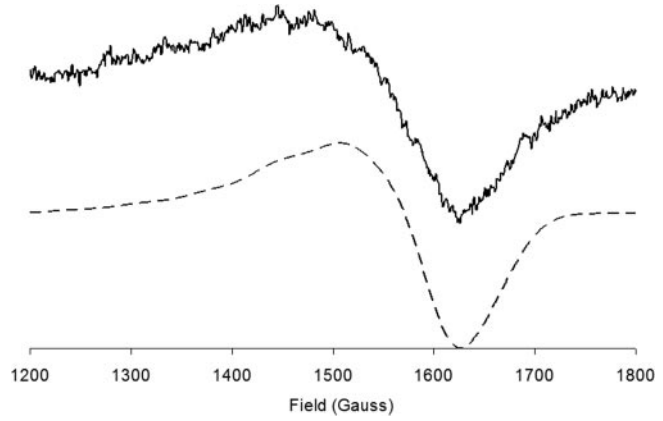

FIGURE 3. **Half-field (g ~ 4) EPR spectrum of Aβ 1-28 at a Cu^{2+}/peptide molar ratio 0.6:1.** Spectra where acquired in PBS, pH 7.4, at 120 K, showing resonance at g ~ 4. Spectrometer and settings were as follows: Bruker ESP380E, microwave frequency 9.424 GHz, microwave power 26.4 milliwatts, modulation frequency 100 kHz, modulation amplitude 5.0 G, receiver gain 1×10^5, scan time 84 s, time constant 40 ms, 26 scans. The spectrum was base line-corrected by subtraction of a spectrum obtained under identical conditions of a quartz tube from the same batch containing PBS, pH 7.4. *Broken line*, SOPHE simulation (20) of the spectrum. Spin-Hamiltonian parameters are given in supplementary Table 1. A simulation, using the same spin-Hamiltonian parameters but with a smaller line width in order to delineate the positions of the Cu^{2+} hyperfine resonances, is shown in supplemental Fig. 1.

range of Cu^{2+}/peptide molar ratios 0.3–1:1. Only mononuclear spectra were observed, similar to those previously published by Tickler *et al.* (4). There were no indications of the broad resonance at g ~ 2 characteristic of the binuclear Cu^{2+} center or for resonances near g ~ 4, even at spectrometer settings where the g ~ 4 resonances were clearly observed in the unmodified peptides. Fig. 2*d* shows the mononuclear spectra obtained with WT Aβ 1-42 at a Cu^{2+}/peptide molar ratio of 0.1:1 and the similarly mononuclear spectra of His-τ-Me obtained at a Cu^{2+}/peptide molar ratio of 1:1 (Fig. 2*e*).

High pressure immobilized affinity chromatography was employed to ascertain if the methylation of the imidazole side chains had a significant effect on the relative Cu^{2+} binding affinity compared with WT Aβ 1-42. The strength of peptide-metal ion interactions is usually assessed as a function of the pH required to elute the various peptides from a Cu^{2+}-loaded immobilized metal ion affinity chromatography column. However, we were unable to elute any of the peptides from the Cu^{2+}-charged immobilized metal ion affinity chromatography column at pH <2 or by using an imidazole gradient. The peptides could only be eluted by the addition of EDTA to the eluting buffer, indicating that all peptides had a very high affinity for Cu^{2+}.

The effect of buffer conditions on Aβ-Cu^{2+} coordination was investigated by acquiring spectra of Aβ 1–28 in pH 7.4 ethylmorpholine buffer over a range of Cu^{2+}/peptide molar ratios, recreating the conditions of Syme *et al.* (7) (supplemental Fig. 1). At Cu^{2+}/peptide molar ratios of 0.1:1 and 1:1, only mononuclear spectra where observed. Spectra in the g ~ 2 region were identical to those reported at Cu^{2+}/peptide ratios of ≤1:1 by Syme *et al.* (7). The broad line near g ~ 2 was not observed, even at Cu^{2+} concentrations and spectrometer settings that yielded these resonances in PBS. Therefore, Aβ-Cu^{2+} complexes in an ethylmorpholine buffer do not generate the specific binuclear Cu^{2+} centers observed in PBS at Cu^{2+}/peptide molar ratios of ≤1:1.

Observation of the His Bridge as Deduced from EPR Spectroscopy—The EPR spectra due to pairs of Cu^{2+} ions separated by distances of around 3–7 Å were first described 30 years ago (12). These spectra arise from the exchange and/or dipolar coupling of two Cu^{2+} ions, each with spin $S = ½$, to give a singlet state ($S = 0$) and a triplet state ($S = 1$). "Allowed" electron spin transitions within the triplet state,

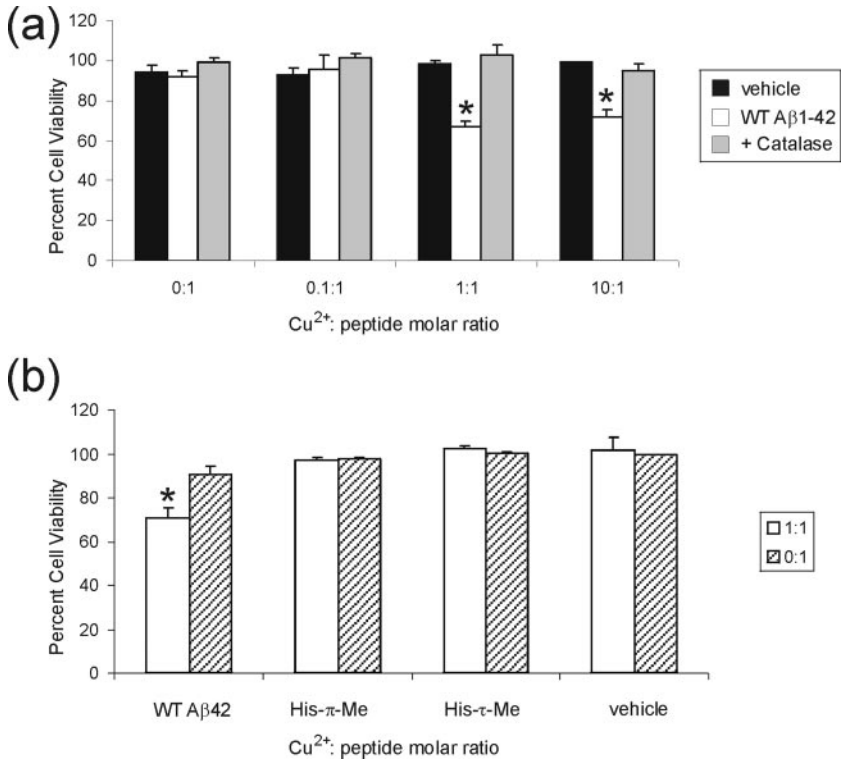

FIGURE 4. **Toxicity of WT Aβ 1-42 and variant peptides coordinated to Cu^{2+}.** Primary cortical neurons were grown at low density (1.25×10^5 cells/cm^2) for 5 days, and the viability of these cells following peptide treatment was determined by measuring the inhibition of MTS reduction. Cortical neurons were treated with 5 μM peptide for 96 h in serum-free media. *a*, WT Aβ 1-42 at a range of Cu^{2+}/peptide molar ratios (□), vehicle control (■), WT Aβ 1-42 at a range of Cu^{2+}/peptide molar ratios plus catalase (▨). *b*, WT Aβ 1-42, His-τ-Me, and His-π-Me at a final concentration of 5 μM at Cu^{2+}/peptide molar ratios of 0:1 (▨) and 1:1 (□). Data are shown as mean ± S.E. Statistical comparisons between groups were done using Student's *t* test. $p < 0.05$ *versus* vehicle; each experiment was carried out in triplicate.

where the magnetic spin quantum number M changes by 1 ($\Delta M = \pm 1$), occur near g ~ 2, whereas "forbidden" or "half-field" transitions, where $\Delta M = \pm 2$, occur near g ~ 4. Thus, the broad line at g ~ 2 and the resonance at g ~ 4 are diagnostic for a pair of Cu^{2+} ions coupled by exchange and/or dipolar interactions. Provided that second order exchange is negligible, the zero field splitting of the triplet state is due to dipolar interactions alone, and its magnitude depends on $1/R^3$, where R is the internuclear distance. The distance between the Cu^{2+} ions can be calculated from the zero field splitting of the triplet state and can be estimated by the use of computer simulations.

The measurements at 2.5 K show that antiferromagnetic exchange interactions are $\ll 10\ cm^{-1}$ and therefore that the effect of second order exchange on the zero field splitting of the triplet state can be neglected. The *broken line spectra* shown in Figs. 2 and 3 were simulated, assuming that the zero field splitting of the triplet state is due to dipolar coupling alone. The parameters giving the best fits are listed in supplemental Table 1. The fits were obtained by successively varying the geometrical and spin Hamiltonian parameters and line widths until agreement between the field positions of peaks in the experimental and computed spectra was within ~10 G. Differences between simulated and experimental spectra are due to line width variations, and in the case of the g ~ 2 spectra to there being an equilibrium between different Cu^{2+}-bound states of the peptide, with the simulation representing the predominant species. The simulation of the g ~ 4 resonance is presented in supplemental Fig. 2 with a smaller line width in order to more clearly delineate the positions of the Cu^{2+} hyperfine peaks. All fitting attempts converged to the same range of parameters required to fit both the $\Delta M = 1$ and $\Delta M = 2$ spectra. The values of $g_{\|} = 2.34 \pm 0.01$ and $g_{\perp} = 2.12 \pm 0.01$ are larger than expected for 2- or 3-nitrogen coordination but indicate that the Cu^{2+} coordination geometry is distorted toward tetrahedral (24).

Therefore, the picture that emerges is of one involving two structurally identical Cu^{2+} sites, probably 3N-coordinated, in a tetrahedrally distorted square planar configuration. The Cu^{2+} ions are 6.2 ± 0.2 Å apart, with axially symmetric g and A matrices, but with the symmetry axes tilted toward the internuclear vector and toward each other by 15 ± 5°. The 6.2 ± 0.2-Å distance between the Cu^{2+} atoms is consistent with our hypothesis that Cu^{2+} coordination by Aβ at 1:1 Cu^{2+}/peptide occurs via a His bridge between two metal centers to generate a structure that resembles the active site of superoxide dismutase 1 (25). The formation of such a bridge is inhibited by the methylation of either of the nitrogen atoms from the imidazole side chain.

Toxic Properties of Aβ-Cu^{2+} Complexes—To ascertain the possible physiological significance of the His bridge, Aβ 1-42 (5 μM) at Cu^{2+}/peptide molar ratios of 0:1, 0.1:1, 1:1, and 10:1 was tested for neurotoxic activity on mouse primary cortical cultures (Fig. 4*a*). Only Aβ 1-42 prepared at a Cu^{2+}/peptide molar ratio of 1:1 and 10:1 showed neurotoxicity at 5 μM, with the 1:1 ratio the most toxic. Toxicity was rescued by the addition of the H_2O_2 scavenging enzyme catalase, indicating that production of ROS is a plausible toxic insult. It therefore appears that conditions leading to the formation of His-bridged Aβ oligomers are associated with metal ion-mediated toxicity.

It has previously been shown that metal-free forms of the similarly methylated Aβ 1-40 peptide are nontoxic (4). To investigate the effect of the loss of the His bridge on the toxicity of the metal-bound form of the Aβ peptide, WT Aβ 1-42, His-τ-Me, and His-π-Me were added to mouse primary cortical cultures at Cu^{2+}/peptide molar ratios of 0:1 and 1:1 (Fig. 4*b*). Under these conditions, the WT Aβ 1-42 at a Cu^{2+}/peptide molar ratio of 1:1 reduced cell viability to ~70% as compared with the vehicle. In contrast, both His-τ-Me and His-π-Me were not toxic. The EPR data show that no His bridge was induced by Cu^{2+} in either His-τ-Me or His-π-Me at Cu^{2+}/peptide molar ratios of ≤1:1. The ability of the Aβ peptide to induce toxicity therefore correlates with the formation of the His-bridged dimers of Aβ as observed by EPR.

Cu^{2+} Modulation of Aβ Amyloid Formation—Our data suggest that the ability of Aβ 1-42 to form a His-bridged Cu^{2+}-induced dimer was required for metal-mediated toxicity. In order to determine if there is a correlation between the ability of the peptides to form amyloid material

and this toxic species, WT Aβ 1-42, His-π-Me, and His-τ-Me were incubated at 37 °C for 2 h at Cu^{2+}/peptide molar ratios of 0:1 to 25:1. The amyloid content was assessed by use of ThT fluorescence, and the morphology was assessed by electron microscopy. In the absence of added Cu^{2+}, all peptides showed an increase in ThT fluorescence, indicating the formation of amyloid material (Fig. 5). Comparable ThT intensities and peptide aggregate morphologies where observed after 24 h of incubation (data not shown). It is interesting to note that His-π-Me produced a 2-fold increase in ThT signal over both WT Aβ 1-42 and His-τ-Me. This increase in signal may be due to subtle changes in the morphology of the fibril leading to a greater binding capacity for ThT or an increase in the total amount of amyloid material. As the Cu^{2+} concentration was raised, all three peptides displayed a loss in amyloidogenic material, evident as a decrease in ThT fluorescence. The Cu^{2+}-induced shifts in the aggregation profile from amyloid material to amorphous aggregates centered close to a Cu^{2+}/peptide molar ratio of 1:1 and were evident for all three peptides. Electron microscopy morphological analysis of all aggregates (data not shown) demonstrated that the decrease in ThT signal corresponded to a loss in fibrillar material and a gain in amorphous aggregate material ranging in size from 10 nm to 1 μm. His-π-Me does display a small amount of ThT fluorescence even in the presence of high Cu^{2+} concentration (Fig. 5), and concurrently small fibrillar-like aggregates were observed by electron microscopy (data not shown). Nevertheless, all three peptides displayed a loss in amyloid material as the Cu^{2+} concentration rose, and it appears that Cu^{2+}-induced aggregation of Aβ is not dependent on the ability of the peptide to form a His bridge but on its ability to coordinate the initial Cu^{2+}. It is also clear that conditions promoting the formation of amyloid material do not lead to metal ion-mediated toxicity. CD spectra were recorded for all peptides to determine whether the modifications significantly altered the structural properties of the peptide in the presence and absence of Cu^{2+}. All three unaged peptides formed β-sheet structures in the presence of Cu^{2+}, with the two modified peptides having a greater β-sheet propensity than the WT peptide (supplemental Fig. 3).

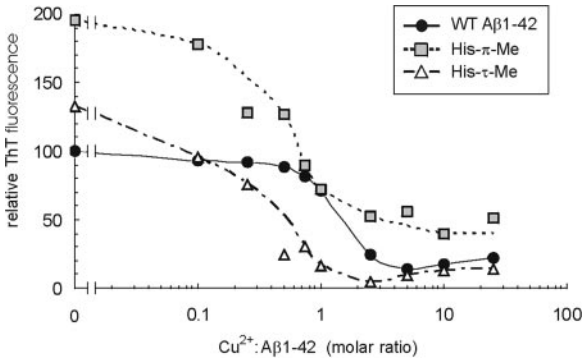

FIGURE 5. **Aggregation properties of Aβ 1-42 at various Cu^{2+}/peptide molar ratios.** Shown is amyloid formation by WT Aβ 1-42 (●), His-τ-Me (△), and His-π-Me (▨), as a function of Cu^{2+} concentration, as monitored by ThT fluorescence. 10 μM samples were aged at 37 °C for 2 h with agitation at 200 rpm. The experiment was repeated on three occasions, showing similar results.

Cu^{2+} Modulation of Aβ Lipid Interactions—Previous work by our group (4, 21, 26) and others (13–17) has indicated that the primary toxic mechanism of Aβ requires an interaction with the plasma membrane of cells. In order to assess the ability of Aβ 1-42 and the variant peptides to penetrate the lipid membrane, the change in fluidity of the acyl-chain region of LUVs was monitored by the anisotropy of DPH. DPH is known to intercalate axially to the acyl-chain region of a lipid bilayer, and it reports on the flexibility of this hydrophobic environment (27). Both aged and unaged WT Aβ 1-42 at Cu^{2+}/peptide molar ratios of 0:1 and 1:1, corresponding to the absence or presence of the His bridge, were allowed to associate with LUVs composed of 50% PC and 50% PS. The steady-state anisotropy of DPH was then measured after 20 min of incubation (Fig. 6). When unaged WT Aβ 1-42 was allowed to interact with the lipid membrane, there was little change in the fluidity of the acyl-chain region over buffer alone (Fig. 6*a*). However, upon aging for 24 h, which resulted in the formation of amyloid material, there was a large decrease in the fluidity of the acyl-chain region as observed by the increase in anisotropy, representing a perturbation of the membrane bilayer by the amyloidogenic material. The nonamyloidogenic Cu^{2+} aggregates produced at a Cu^{2+}/peptide ratio of 1:1 did not by contrast perturb this region of the bilayer. A similar pattern of lipid perturbation was observed with His-π-Me and His-τ-Me, where only the presence of amyloid material leads to a perturbation of the acyl-chain region of the membrane. It is notable that Cu^{2+} aggregates created by each of the variant peptides do not lead to a change in the fluidity of the acyl-chain region of the membrane. Whereas the magnitude of the fluorescence signal of DPH was slightly quenched by Cu^{2+} (<10–15%), the anisotropy of the fluorophore was not affected by the presence of the metal ion, since the signal recorded in buffer only is identical in the presence or absence of additional Cu^{2+} ions. Also, because anisotropy is a ratio of the intensity of the polarized light to the total light, it varies only with the motility of the fluorophore. These observations would suggest that mechanical interference of the acyl-chain region of the lipid membrane by the Aβ 1-42 peptide does not contribute to metal ion-mediated toxicity.

To ascertain if Aβ and Aβ-Cu^{2+} complexes were interacting with the head group region of the lipid membrane, experiments were carried out by ^{31}P magic angle spinning solid-state NMR. The ^{31}P solid-state NMR spectra of the phospholipid head group of the LUV showed a broad

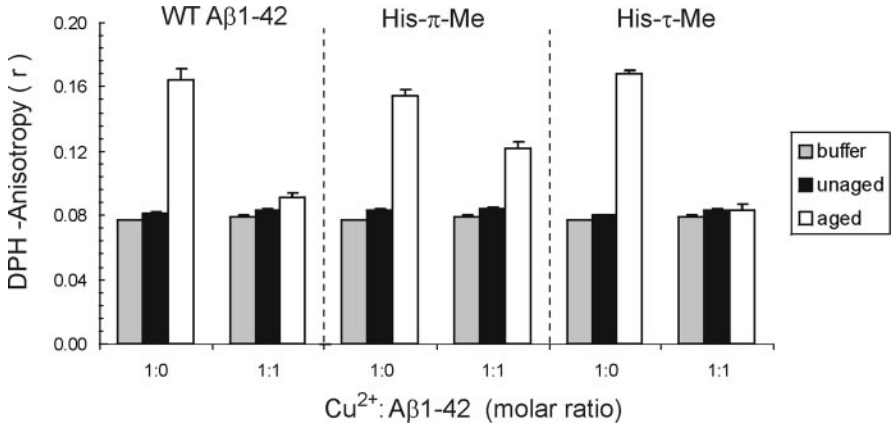

FIGURE 6. **Perturbation of the acyl-chain region of a lipid bilayer by Aβ 1-42.** Shown is the effect of WT Aβ 1-42, His-π-Me, and His-τ-Me at Cu^{2+}/peptide molar ratios of 0:1 and 1:1, for both unaged (■) and aged peptide (□) and buffer alone (▨) on the anisotropy (*r*) of DPH in synthetic LUVs (50% PC, 50% PS). Data are shown as mean ± S.E.; each experiment was carried out in triplicate.

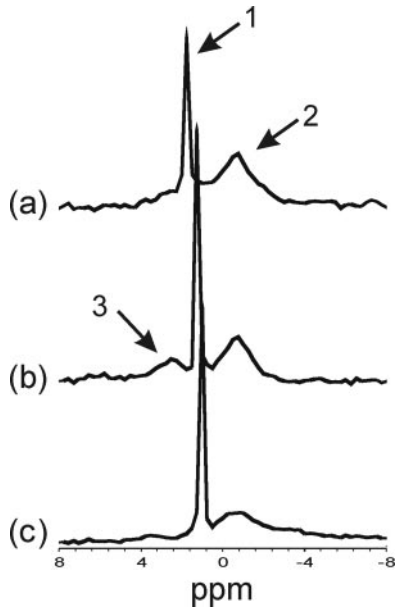

FIGURE 7. **^{31}P magic angle spinning NMR spectra of LUV in the presence of WT Aβ 1-42 and Cu^{2+}.** Spectra were acquired in PBS, pH 7.4. Shown are lipid alone (*a*), with WT Aβ 1-42 added at a lipid/peptide ratio of 30:1 (*b*), and with WT Aβ 1-42 in the presence of equimolar Cu^{2+} at a lipid/peptide ratio of 30:1 (*c*). Peak labels are as follows. *1*, phosphate buffer resonance ~1.5 ppm. *2*, phospholipid head group of LUV −0.75 ppm. *3*, lipid-peptide-associated phase 2.51 ppm.

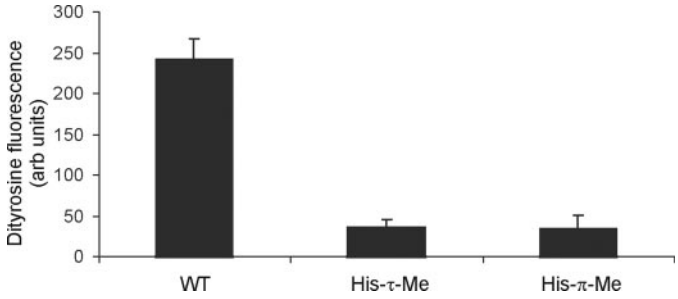

FIGURE 8. **Formation of dityrosine Aβ adducts.** Shown are WT Aβ 1-42, His-π-Me, and His-τ-Me. 10 μM peptide was incubated at 37 °C with agitation at 200 rpm for 2 h at a Cu^{2+}/peptide molar ratio of 1:1 in the presence of 250 μM H_2O_2. Data are shown as mean ± S.E.; each experiment was carried out in triplicate.

resonance at −0.75 ppm (Fig. 7*a*, *arrow 2*); the addition of Aβ 1-42 resulted in the appearance of a new resonance at 2.51 ppm (Fig. 7*b*, *arrow 3*). The appearance of the second peak indicated the formation of a lipid-peptide-associated phase. When Aβ 1-42-coordinating Cu^{2+} was added to LUV, the Aβ 1-42-associated lipid signal was reduced significantly and broadened (Fig. 7*c*), consistent with the paramagnetic Cu^{2+} being bound to Aβ 1-42 and in close association with the phospholipid head group. The Cu^{2+} bound to Aβ 1-42 caused paramagnetic relaxation of the peptide-bound peak and T_2 broadening of peaks due to both PC and PS lipids. This indicated that the Cu^{2+} was interacting preferentially with the Aβ-phospholipid associated phase rather than the nonassociated phase. This supports our previous cortical cell culture studies, where lipid-peptide binding appears to be crucial for cell toxicity and suggests that phospholipid head group interaction plays an important role in the pathway for neurotoxicity (4, 21, 26, 28). It is also worth noting that there is a small shift in the peak due to the phosphate buffer upon the addition of Aβ, from 1.76 to 1.26 ppm, with a further shift to 1.00 ppm upon the addition of Cu^{2+}. Such shifts are consistent with the concept that the buffer plays a role in determining the structure of the peptide as outlined above.

Dityrosine Formation Correlates with the Ability to Form a His Bridge—Tyr^{10} is a critical residue in the production of ROS by Aβ (29), and the resulting formation of dityrosine adducts has been suggested to play a role in Aβ aggregation and neurotoxicity (22, 29). Dityrosine adducts of Aβ are formed as a by-product when the peptide is incubated in the presence of Cu^{2+} and H_2O_2 (22, 29). The addition of H_2O_2 strongly promotes dityrosine cross-linking via the increased production of ROS (22, 29). The role of the His bridge in the generation of dityrosine adducts was assessed by assaying the formation of dityrosine by WT Aβ 1-42, His-π-Me, and His-τ-Me at a Cu^{2+}/peptide molar ratio of 1:1 in the presence of 250 mM H_2O_2 (Fig. 8). In comparison with WT Aβ 1-42, His-π-Me and His-τ-Me showed a marked decrease in the ability to generate dityrosine adducts (Fig. 8). This lack of dityrosine adducts reflects a loss in the ability to form the His bridge between Cu^{2+} atoms. Since tyrosine radicals are relatively short lived, it is likely that the formation of a His bridge between two Cu^{2+} atoms bound to two different Aβ peptides facilitates the covalent cross-linking by two tyrosine radicals to generate a dityrosine moiety. The ability of the Aβ peptides to form dityrosine adducts (Fig. 8), therefore, correlates with metal-dependent toxicity, as shown in Fig. 4*b*.

Cu^{2+} Modulation of Aβ-induced Lipid Peroxidation—Lipid peroxidation is a well established mechanism of cellular injury and an indicator of oxidative stress that has been implicated in the pathogenesis of AD (15). Peroxidation of unsaturated fatty acids produces lipid peroxides that are unstable and decompose to form a series of compounds, including reactive carbonyl compounds. To assess whether Aβ-Cu^{2+} complexes can oxidize lipid membranes, we have used a colorimetric assay to monitor the formation of malondialdehyde and 4-hydroxyalkenals, which are generated by the peroxidation of unsaturated phospholipids. WT Aβ 1-42, His-τ-Me, and His-π-Me at Cu^{2+}/peptide molar ratios of 0:1 and 1:1 were incubated with 1 mM 50% PC, 50% PS LUVs for 24 h in the presence of 10 mM ascorbate, which is present to act as a reductant to initiate redox cycling of the Cu^{2+} (30). Lipids incubated in an oxygen atmosphere undergo some degree of peroxidation in the presence of free Cu^{2+} and ascorbate. However, in the presence of WT Aβ 1-42 at a Cu^{2+}/peptide molar ratio of 1:1, there was a significant increase in lipid peroxidation compared with the vehicle (Fig. 9*a*). In contrast, lipid peroxidation was attenuated by both His-π-Me and His-τ-Me, consistent with the lower neurotoxicity displayed by these peptides at the 1:1 ratio. The metal-attenuating compound clioquinol (CQ) can inhibit Aβ toxicity (29) and amyloid deposition in transgenic mice (31). In a small phase II clinical trial, CQ was efficacious in moderately affected AD subjects (32). CQ coordinates Cu^{2+} with a ligand/metal stoichiometry of 2:1 (33), and we show here that it can inhibit the lipid peroxidation induced by the WT Aβ-Cu^{2+} complex (Fig. 9*b*).

DISCUSSION

We have previously postulated that one consequence of Cu^{2+} coordination by Aβ is the formation of a His bridge between two Cu^{2+} atoms (Fig. 1) (2, 4), a concept that has been challenged (6–8). Our EPR data presented here and elsewhere (2, 4) provide strong support for the existence of a 6.2 ± 0.2-Å binuclear Cu^{2+} center, consistent with the occurrence of a His bridge, at Cu^{2+}/peptide molar ratios in the range 0.5–1.0:1 for Aβ 1–28, Aβ 1-40, and Aβ 1-42 in PBS. The absence of any evidence for Cu^{2+}-bridged dimers at Cu^{2+}/peptide molar ratios of 1:1 with the His-τ-Me and His-π-Me establishes the importance of the imidazole side chain in dimer formation. The broad EPR signals reported here have not been reported in a number of other EPR studies of Aβ-Cu^{2+} interactions (6–8). This discrepancy is due to differences in buffer conditions and the mode of presentation of Cu^{2+} to the Aβ peptide; no two studies have used the same conditions.

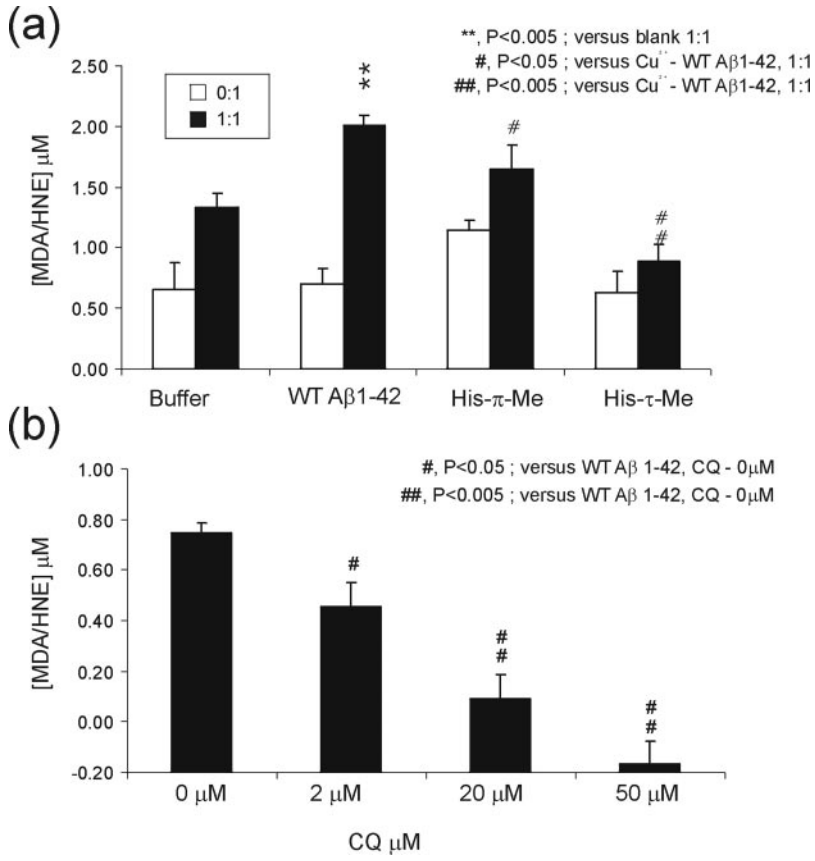

FIGURE 9. **Lipid peroxidation of synthetic LUVs.** *a*, 1 mM lipid was incubated with 10 μM peptide and 10 μM ascorbate at Cu^{2+}/peptide ratios of 0:1 (□) and 1:1 (■) for 24 h at 37 °C. *b*, 1 mM lipid was incubated with 10 μM WT peptide and 10 mM ascorbate at Cu^{2+}/peptide ratios of 1:1 for 24 h at 37 °C. CQ was added at a final concentration of 2, 20, and 50 μM in Me_2SO. Me_2SO was at a final concentration of 1% and accounts for the lower observed level of lipid peroxidation. Lipid peroxidation was determined via a colorimetric assay that measures the concentration of peroxidation by-products malondialdehyde (*MDA*) and 4-hydroxyalkenals (*HNE*). Data are shown as mean ± S.E. Statistical comparisons between groups were done using Student's *t* test. $p < 0.05$ *versus* vehicle; each experiment was carried out in triplicate.

TABLE 1

Correlation of toxicity with formation of His-bridged structures and membrane binding

Conditions leading to both His bridge formation and membrane interactions increased the Cu^{2+}-mediated neurotoxicity of Aβ peptide and its variants. Membrane interactions are defined as cellular binding, binding/insertion to synthetic lipids in the presence or absence of cholesterol/lipid peroxidation.

Peptides	Toxicity	Cu^{2+} coordination/His bridge formation	Membrane Interactions
Nontoxic Aβ peptides			
Aβ 1-28	Slight (43)	Yes/Yes (2, 3)[a]	Slight (43, 45)
Aβ 1-40 His-τ-Me	No (4)	Yes/No (4)	No (4)
Aβ 1-40 His-π-Me	No (4)	Yes/No (4)	No (4)
Aβ 1-42 His-τ-Me	No (17)[a]	Yes/No[a]	Slight (17)[a]
Aβ 1-42 His-π-Me	No (17)[a]	Yes/No[a]	No (17)[a]
Aβ 1-42 Y10A	Slight (17, 29)	Yes/Unknown (29)	Slight (17)
Toxic Aβ peptides			
Aβ 1-40	Yes (5, 43)	Yes/Yes (4)	Yes (43, 45, 46)
Aβ 1-42	Yes (5, 17, 21, 29, 43)[a]	Yes/Yes[a]	Yes (17, 43)[a]
Aβ 1-42 M35V	Enhanced (21)	Yes/Unknown (21)	Enhanced (21)
Aβ 1-42 Met Ox	Yes (26)	Yes/Unknown (26)	Yes (26)

[a] Data in this paper.

Both Huang *et al.* (34) and Narayanan and Reif (35) have shown that buffer constituents, such as NaCl, have a marked effect on metal-mediated oligomerization of Aβ. We obtained our spectra in PBS at pH ~ 6.9–7.5 and presented Cu^{2+} as $CuCl_2$ (2). In contrast, Syme *et al.* (7) used the nonphysiological ethylmorpholine buffers at pH 7.8 and presented Cu^{2+} as $Cu(NO_3)_2$. When we acquired a Cu^{2+} EPR spectrum at Cu^{2+}/peptide molar ratios of 1:1 in this buffer, we also did not observe line broadening. We have been careful to distinguish between the broad lines due to either His-bridged binuclear Cu^{2+} centers or aggregates and the line broadening of mononuclear spectra that can arise in different ways. Further, the pleiomorphic nature of Aβ is well documented, and it is not surprising that the buffer conditions used will have a profound influence on the observed structural state.

Whereas the mechanism of Aβ toxicity in AD remains unresolved, a general theme is beginning to emerge whereby the interaction of Aβ with lipid membranes is a necessary step in neurotoxicity (13–17). These interactions result in changes in membrane fluidity leading to depolarization and disorder (13), pore/channel formation leading to ion channel formation and disrupted calcium homeostasis (14, 16), lipid peroxidation via membrane-associated free radical formation (15), and cholesterol oxidation (17). H_2O_2 and ROS production has been implicated in the neurotoxicity of Aβ, and the Aβ-Cu^{2+} complexes are able to produce H_2O_2 (36–38). The production of H_2O_2 has been shown to occur during a short burst at the early stages of aggregation, around the time soluble oligomers are being produced (39). In this study, we demonstrated that toxicity to primary cortical neurons correlates with the formation of a His bridge between Cu^{2+} ions, which is populated at equimolar Cu^{2+}/peptide ratios (Figs. 3 and 4). The resulting toxic effect was rescued by the addition of catalase, implicating H_2O_2 generation. A consequence of ROS production is lipid peroxidation, resulting in sub-

sequent cell death, which precedes amyloid plaque formation (15, 40). Supporting this mechanism, we have demonstrated that Aβ 1-42 at Cu^{2+}/peptide molar ratios of 1:1, conditions in which the His bridge was formed, induced lipid peroxidation (Fig. 9). Interestingly, the observed toxicity to primary cortical neurons does not correlate with the ability of the peptides to form amyloid material or to mechanically perturb the acyl-chain region of a lipid membrane, as monitored by the anisotropy of DPH (Figs. 5 and 6). Solid-state NMR studies indicate that the Aβ peptide has an affinity for negatively charged phospholipids (41, 42). Our previous ^{31}P static solid-state NMR data have also shown that metal-bound forms of Aβ increase perturbation of the lipid head groups, mediated through Cu^{2+} binding, compared with the metal-free form (28). Here we demonstrate the appearance of a lipid-Aβ-bound phase and a peptide-free lipid phase (Fig. 7) due to the lipid head group interaction with WT Aβ 1-42. The observation of a lipid-Aβ-bound phase indicated that Aβ and Aβ-Cu^{2+} complexes were able to associate with the lipid membrane head group region and that this association would promote lipid peroxidation.

Conditions that lead to the formation of the His-bridged Aβ oligomers result in the population of a highly toxic species. It follows, therefore, that disruption of this structure would abrogate Aβ toxicity. In agreement with this hypothesis, methylation of the three His residues at either the τ- or π-nitrogen of the imidazole side chain resulted in the elimination of the His bridge at equimolar Cu^{2+}/peptide ratios (Figs. 2 and 3). These modifications rendered the peptide nontoxic (Fig. 4); congruently, a loss in lipid peroxidation activity was observed (Fig. 9*a*). That CQ was able to inhibit the observed lipid peroxidation (Fig. 9*b*) is consistent with this process being a metal-dependent phenomenon, since previously observed data have shown that CQ inhibits Aβ/Cu interactions (31). The loss in toxic activity presumably resulted from the modified Aβ peptides sequestering the redox-active Cu^{2+} away from the lipid environment. Tickler *et al.* (4) have shown previously that His-π-Me- and His-τ-Me-modified Aβ peptides have a lower affinity for lipid membranes, and since ROS are relatively short lived species that react with substrates in their immediate vicinity, less lipid peroxidation is expected and observed for these peptides.

Moreover, eliminating the His bridge also affected the formation of dityrosine adducts (Fig. 8). Tyr^{10} is critical in the redox cycling of Cu^{2+}-associated ROS production by Aβ-Cu^{2+} (29). A by-product of the redox reactions is that two tyrosine radicals can react to form dityrosine adducts. The formation of dityrosine adducts by both His-π-Me and His-τ-Me Aβ was severely inhibited (Fig. 8), correlating with the decrease in lipid peroxidation (Fig. 9) and subsequent toxicity (Fig. 4). This is consistent with a role for either the tyrosine radical or dityrosine in metal-mediated toxicity.

A survey of the literature shows that variations to the Aβ peptide sequence that ablate lipid binding cause a decrease in Aβ neurotoxicity (Table 1). Aβ 1-28, which is capable of binding to lipids, although weakly, has been reported to show a small degree of toxicity (43). Methylation of the His residues at either the π- or τ-nitrogen of the imidazole side chain of Aβ 1-40/42 results in a loss in lipid binding and toxicity as well as a loss in the ability to form the His bridge (4). By contrast, Aβ 1-42 containing a M35V mutation shows an increase in toxicity over the WT peptide and displays a higher affinity for lipid membranes (21). In addition, Aβ 1-42 with an oxidized Met^{35} is unable to penetrate the lipid membrane but is able to bind to the surface and induce toxicity (26). These results, together with the data presented here, lead to a model whereby binding of Aβ to the surface of a lipid membrane is required to cause Cu^{2+}-induced toxicity. Taken with the results presented above, the toxic Aβ-Cu^{2+} species requires the formation of the His bridge and imparts its toxic effect via the association with lipids and the generation of ROS, resulting in lipid peroxidation and subsequent cell death. The lipid peroxidation can be inhibited by the use of the metal-attenuating compound CQ, which can disaggregate metal-induced aggregates and retard fibril growth (44) and inhibit amyloid deposition in transgenic mice (31) and was efficacious in a phase II clinical trial on a severely affected AD group (32). Therefore, strategies aimed at inhibiting the formation of His-bridged Aβ-Cu^{2+} complexes, thereby preventing metal-induced Aβ oligomer formation and consequent production of ROS, would limit the oxidative stress associated with AD and be of therapeutic benefit.

Acknowledgment—We thank Stephen Bottomley for access to the CD spectrometer.

REFERENCES

1. Bush, A. I. (2003) *Trends Neurosci.* **26,** 207–214
2. Curtain, C. C., Ali, F., Volitakis, I., Cherny, R. A., Norton, R. S., Beyreuther, K., Barrow, C. J., Masters, C. L., Bush, A. I., and Barnham, K. J. (2001) *J. Biol. Chem.* **276,** 20466–20473
3. Curtain, C. C., Ali, F. E., Smith, D. G., Bush, A. I., Masters, C. L., and Barnham, K. J. (2003) *J. Biol. Chem.* **278,** 2977–2982
4. Tickler, A., Smith, D., Ciccotosto, G., Tew, D., Curtain, C. C., Carrington, D., Masters, C. L., Bush, A. I., Cherny, R. A., Cappai, R., Wade, J., and Barnham, K. J. (2005) *J. Biol. Chem.* **280,** 13355–13363
5. Huang, X., Cuajungco, M. P., Atwood, C. S., Hartshorn, M. A., Tyndall, J. D., Hanson, G. R., Stokes, K. C., Leopold, M., Multhaup, G., Goldstein, L. E., Scarpa, R. C., Saunders, A. J., Lim, J., Moir, R. D., Glabe, C., Bowden, E. F., Masters, C. L., Fairlie, D. P., Tanzi, R. E., and Bush, A. I. (1999) *J. Biol. Chem.* **274,** 37111–37116
6. Antzutkin, O. N. (2004) *Magn. Reson. Chem.* **42,** 231–246
7. Syme, C. D., Nadal, R. C., Rigby, S. E., and Viles, J. H. (2004) *J. Biol. Chem.* **279,** 18169–18177
8. Karr, J. W., Kaupp, L. J., and Szalai, V. A. (2004) *J. Am. Chem. Soc.* **126,** 13534–13538
9. Karr, J. W., Akintoye, H., Kaupp, L. J., and Szalai, V. A. (2005) *Biochemistry* **44,** 5478–5487
10. Zirah, S., Kozin, S. A., Mazur, A., Blond, A., Cheminant, M., Segalas-Milazzo, I., Debey, P., and Rebuffat, S. (2006) *J. Biol. Chem.* **281,** 2151–2161
11. Ohtsu, H., Shimazaki, Y., Odani, A., Yamauchi, O., Mori, W., Itoh, S., and Fukuzumi, S. (2000) *J. Am. Chem. Soc.* **122,** 5733–5741
12. Smith, T. D., and Pilbrow, J. R. (1974) *Coord. Chem. Rev.* **13,** 173–278
13. Eckert, G. P., Wood, W. G., and Muller, W. E. (2005) *Subcell. Biochem.* **38,** 319–337
14. Kagan, B. L., Hirakura, Y., Azimov, R., Azimova, R., and Lin, M. C. (2002) *Peptides* **23,** 1311–1315
15. Butterfield, D. A., and Boyd-Kimball, D. (2004) *Brain Pathol.* **14,** 426–432
16. Kawahara, M. (2004) *Curr. Alzheimer Res.* **1,** 87–95
17. Puglielli, L., Friedlich, A. L., Setchell, K. D., Nagano, S., Opazo, C., Cherny, R. A., Barnham, K. J., Wade, J. D., Melov, S., Kovacs, D. M., and Bush, A. I. (2005) *J. Clin. Invest.* **115,** 2556–2563
18. Tickler, A. K., Barrow, C. J., and Wade, J. D. (2001) *J. Pept. Sci.* **7,** 488–494
19. Wertz, J. E., Orton, J. W., and Auzins, P. (1961) *Discuss. Faraday Soc.* **31,** 140–150
20. Hanson, G. R., Gates, K. E., Noble, C. J., Griffin, M., Mitchell, A., and Benson, S. (2004) *J. Inorg. Biochem.* **98,** 903–916
21. Ciccotosto, G. D., Tew, D., Curtain, C. C., Smith, D., Carrington, D., Masters, C. L., Bush, A. I., Cherny, R. A., Cappai, R., and Barnham, K. J. (2004) *J. Biol. Chem.* **279,** 42528–42534
22. Atwood, C. S., Perry, G., Zeng, H., Kato, Y., Jones, W. D., Ling, K. Q., Huang, X., Moir, R. D., Wang, D., Sayre, L. M., Smith, M. A., Chen, S. G., and Bush, A. I. (2004) *Biochemistry* **43,** 560–568
23. Peisach, J., and Blumberg, W. E. (1974) *Arch. Biochem. Biophys.* **165,** 691–708
24. Sakaguchi, U., and Addison, A. W. (1979) *J. Chem. Soc. Dalton Trans.*, 600–608
25. Parge, H. E., Hallewell, R. A., and Tainer, J. A. (1992) *Proc. Natl. Acad. Sci. U. S. A.* **89,** 6109–6113
26. Barnham, K. J., Ciccotosto, G. D., Tickler, A. K., Ali, F. E., Smith, D. G., Williamson, N. A., Lam, Y. H., Carrington, D., Tew, D., Kocak, G., Volitakis, I., Separovic, F., Barrow, C. J., Wade, J. D., Masters, C. L., Cherny, R. A., Curtain, C. C., Bush, A. I., and Cappai, R. (2003) *J. Biol. Chem.* **278,** 42959–42965
27. Müller, W. E., Kirsch, C., and Eckert, G. P. (2001) *Biochem. Soc. Trans.* **29,** 617–623
28. Lau, T. L., Ambroggio, E. E., Tew, D. J., Cappai, R., Masters, C. L., Fidelio, G. D., Barnham, K. J., and Separovic, F. (2005) *J. Mol. Biol.*, **356,** 759–770
29. Barnham, K. J., Haeffner, F., Ciccotosto, G. D., Curtain, C. C., Tew, D., Mavros, C., Beyreuther, K., Carrington, D., Masters, C. L., Cherny, R. A., Cappai, R., and Bush, A. I.

(2004) *FASEB J.* **18,** 1427–1429
30. Opazo, C., Barría, M. I., Ruiz, F. H., and Inestrosa, N. C. (2003) *Biometals* **16,** 91–98
31. Cherny, R. A., Atwood, C. S., Xilinas, M. E., Gray, D. N., Jones, W. D., McLean, C. A., Barnham, K. J., Volitakis, I., Fraser, F. W., Kim, Y., Huang, X., Goldstein, L. E., Moir, R. D., Lim, J. T., Beyreuther, K., Zheng, H., Tanzi, R. E., Masters, C. L., and Bush, A. I. (2001) *Neuron* **30,** 665–676
32. Ritchie, C. W., Bush, A. I., Mackinnon, A., Macfarlane, S., Mastwyk, M., MacGregor, L., Kiers, L., Cherny, R., Li, Q. X., Tammer, A., Carrington, D., Mavros, C., Volitakis, I., Xilinas, M., Ames, D., Davis, S., Beyreuther, K., Tanzi, R. E., and Masters, C. L. (2003) *Arch. Neurol.* **60,** 1685–1691
33. Di Vaira, M., Bazzicalupi, C., Orioli, P., Messori, L., Bruni, B., and Zatta, P. (2004) *Inorg. Chem.* **43,** 3795–3797
34. Huang, X. D., Atwood, C. S., Moir, R. D., Hartshorn, M. A., Vonsattel, J. P., Tanzi, R. E., and Bush, A. I. (1997) *J. Biol. Chem.* **272,** 26464–26470
35. Narayanan, S., and Reif, B. (2005) *Biochemistry* **44,** 1444–1452
36. Opazo, C., Huang, X., Cherny, R. A., Moir, R. D., Roher, A. E., White, A. R., Cappai, R., Masters, C. L., Tanzi, R. E., Inestrosa, N. C., and Bush, A. I. (2002) *J. Biol. Chem.* **277,** 40302–40308
37. Behl, C., Davis, J. B., Lesley, R., and Schubert, D. (1994) *Cell* **77,** 817–827
38. Huang, X., Atwood, C. S., Hartshorn, M. A., Multhaup, G., Goldstein, L. E., Scarpa, R. C., Cuajungco, M. P., Gray, D. N., Lim, J., Moir, R. D., Tanzi, R. E., and Bush, A. I. (1999) *Biochemistry* **38,** 7609–7616
39. Tabner, B. J., El-Agnaf, O. M., Turnbull, S., German, M. J., Paleologou, K. E., Hayashi, Y., Cooper, L. J., Fullwood, N. J., and Allsop, D. (2005) *J. Biol. Chem.* **280,** 35789–35792
40. Praticó, D., Uryu, K., Leight, S., Trojanoswki, J. Q., and Lee, V. M. (2001) *J. Neurosci.* **21,** 4183–4187
41. Bokvist, M., Lindström, F., Watts, A., and Gröbner, G. (2004) *J. Mol. Biol.* **335,** 1039–1049
42. Bonev, B., Watts, A., Bokvist, M., and Gröbner, G. (2001) *Phys. Chem. Chem. Phys.* **3,** 2904–2910
43. Subasinghe, S., Unabia, S., Barrow, C. J., Mok, S. S., Aguilar, M. I., and Small, D. H. (2003) *J. Neurochem.* **84,** 471–479
44. Raman, B., Ban, T., Yamaguchi, K. I., Sakai, M., Kawai, T., Naiki, H., and Goto, Y. (2005) *J. Biol. Chem.* **280,** 16157–16162
45. Ji, S.-R., Wu, Y., and Sui, S. (2002) *J. Biol. Chem.* **277,** 6273–6279
46. Avdulov, N. A., Chochina, S. V., Igbavboa, U., Ohare, E. O., Schroeder, F., Cleary, J. P., and Wood, W. G. (1997) *J. Neurochem.* **68,** 2086–2091

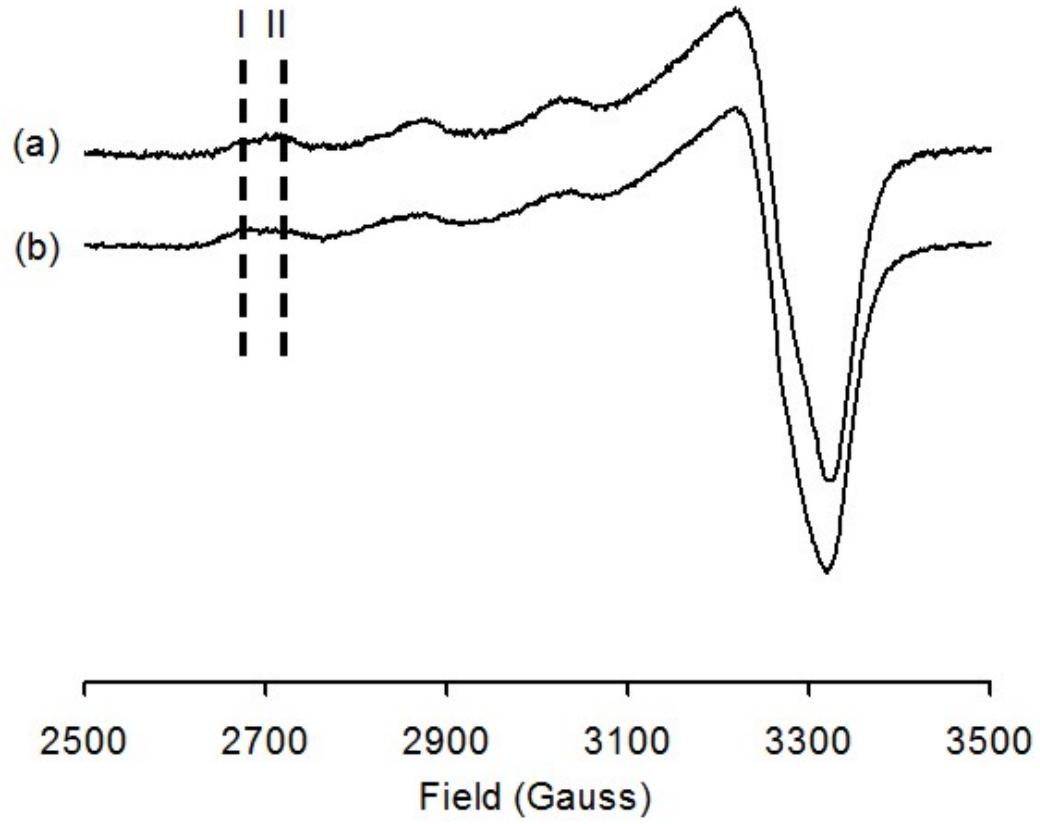

Supplementary Fig 1 - EPR spectra of Aβ1-28 ethylmorpholine buffer. Spectra where acquired at pH 7.4 at 120 K (a) Cu^{2+}:peptide molar ratio of 0.5:1, (b) Cu^{2+}:peptide molar ratio of 1:1. Additional components I and II previously observed (7) shown by broken lines. Note the proportions of I and II are changed as the Cu^{2+}:peptide molar ratio is increased. Spectrometer and settings; Bruker ESP380E, microwave frequency 9.425 GHz, microwave power 4.18 mW, modulation frequency 100 KHz, modulation amplitude 4.0 G, receiver gain 1 x 10^5, scan time 168 s, time constant 164 ms, single scan.

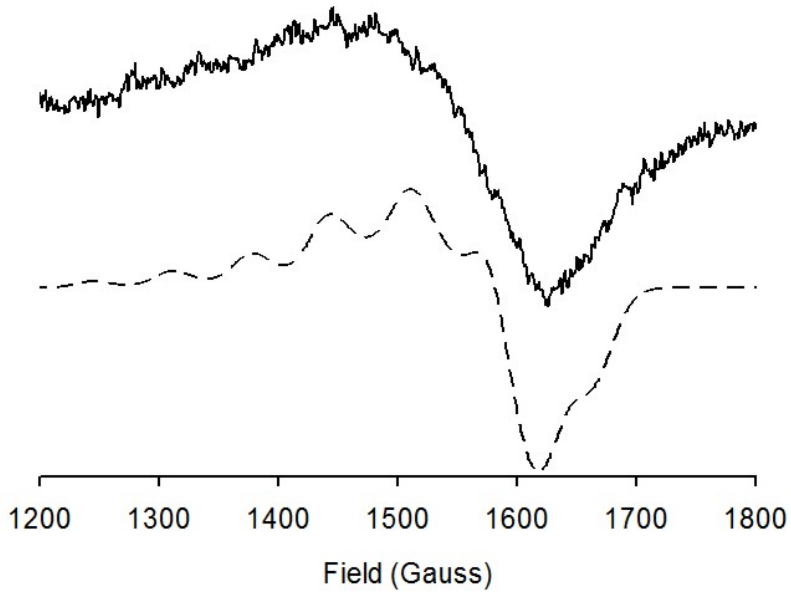

Supplementary Fig 2 - High resolution simulation of half-field resonance. Full line: experimental spectrum of Aβ1-28 in the $g \sim 4$ region as in Figure 3 of main text. Broken line: simulated spectrum using the same spin Hamiltonian parameters as for Figure 3, but with a reduced linewidth in order to more clearly delineate the positions of the Cu^{2+} hyperfine peaks.

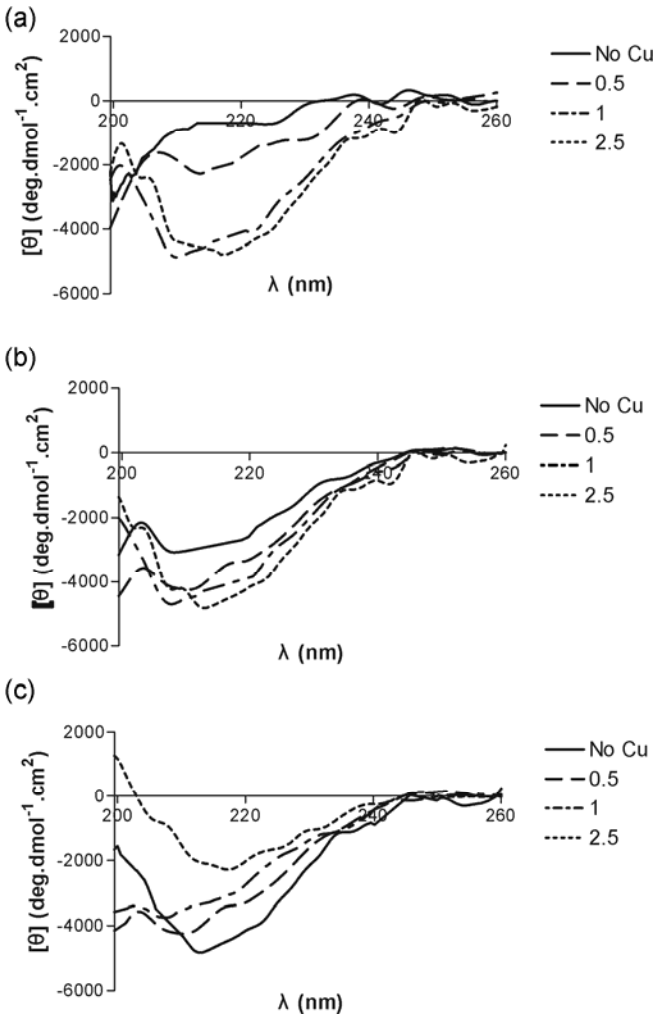

Supplementary Fig 3. CD spectra of Cu^{2+} being titrated into PBS solutions of (a) WT Aβ1-42 (b) His-π-Me Aβ1-42 and (c) His-τ-Me Aβ1-42. All peptides form β-sheet structures upon addition of Cu^{2+}, with the modified peptides having a higher tendency than WT Aβ1-42.

Supplementary Table 1
Spin Hamiltonian parameters for simulated spectra shown in Figures 2a- c and Figure 3. Estimated uncertainties are given in parentheses.

	$g_{\parallel}$	$g_{\perp}$	$A_{\parallel}$ (10^{-4} cm^{-1})	$A_{\perp}$ (10^{-4} cm^{-1})	$\sigma_{\parallel}$ (10^{-4} cm^{-1})	$\sigma_{\perp}$ (10^{-4} cm^{-1})
Aβ1-28 mononuclear Cu^{2+} [a]	2.28 ± 0.01	2.06 ± 0.01	175 ± 5	5 ± 5	50 ± 10	40 ± 10
Aβ1-28 binuclear Cu^{2+} centre [b]	2.340 ± 0.01	2.12 ± 0.01	150 ± 5	5 ± 5	40 ± 5	40 ± 50
Aβ1-28 Cu^{2+} aggregate [c]	2.14 ± 0.01		60 ± 10		120 ± 20	

Notes

[a] Figure 2a
[b] Figure 2b and Figure 3. R (distance between Cu^{2+} ions) 6.2 ± 0.2 Å; z axes of $\boldsymbol{g}$ and $\boldsymbol{A}$ of individual ions tilted towards each other and along the internuclear vector by 15 ± 5°. The linewidth quoted is for the $g \sim 2$ spectrum. The $g \sim 4$ spectrum shown in Figure 3 was simulated with a linewidth of 70 x 10^{-4} cm^{-1}, while that of Supplementary Figure 1 was simulated with a linewidth of 35 x 10^{-4} cm^{-1}.
[c] Figure 2c. The simulation is indicative only. Note that the values of g and A used in the simulation approximate the average of the parameters used to simulate the mononuclear spectrum.

Copper-mediated Amyloid-β Toxicity Is Associated with an Intermolecular Histidine Bridge

David P. Smith, Danielle G. Smith, Cyril C. Curtain, John F. Boas, John R. Pilbrow, Giuseppe D. Ciccotosto, Tong-Lay Lau, Deborah J. Tew, Keyla Perez, John D. Wade, Ashley I. Bush, Simon C. Drew, Frances Separovic, Colin L. Masters, Roberto Cappai and Kevin J. Barnham

J. Biol. Chem. 2006, 281:15145-15154.
doi: 10.1074/jbc.M600417200 originally published online April 4, 2006
